water

MDPI

Article

Thermo-Hydro-Mechanical Evolution and Long-Term Stability of Canal Slopes Under Freeze–Thaw Cycles in Cold Regions

Liang Qiao [1], Yadi Min [2], Hongbo Sun [3], Changhong Song [4], Haiqiang Jiang [5,*], Yating Peng [6,*] and Wanying Jin [2,7]

[1] School of Architecture and Civil Engineering, Xihua University, Chengdu 610039, China
[2] School of Water Conservancy and Civil Engineering, Northeast Agricultural University, Harbin 150030, China
[3] Heilongjiang Dingjie Road and Bridge Engineering Co., Ltd., Harbin 150090, China
[4] Heilongjiang Water Resources Investment Group, Harbin 150040, China
[5] Nanjing University (Suzhou) High-Tech Research Institute, Suzhou 215000, China
[6] Department of Transport and Municipal Engineering, Sichuan University of Architectural Technology, Chengdu 610399, China
[7] Beijing Zhongshui Lide Technology Development Co., Ltd. (Shandong Branch), Jinan 250000, China
* Correspondence: hqjiang@neau.edu.cn (H.J.); pengyating0827@163.com (Y.P.)

Abstract

Freeze–thaw cycles frequently cause damage to canal slopes in cold regions, which has become a potential adverse factor leading to slope failure. This study investigates the coupled thermo-hydro-mechanical (THM) behavior and stability evolution of canal slopes under freeze–thaw cycle conditions through integrated physical model tests and numerical simulations. The evolution processes of temperature distribution, maximum frozen depth, unfrozen water content, deformation, and safety factor of canal slopes were evaluated. The results showed that both the maximum frozen depth and deformation increased continuously within a reasonable service life of 20 years. The maximum deformation concentrated in the middle of the slope, and the maximum unfrozen water content on the slope surface decreased by 0.06. The stability of a canal slope is subject to the dual influences of service time and seasonal variations. Overall, the safety factor decreases with the increase in service time. The safety factor is influenced by the degree of slope freezing. Compared to November, the safety factor in March of the following year increases by 0.15. As slope failure initiates at the slope toe, necessary engineering measures must be implemented at the slope toe in the design of canals to maintain slope stability. This research provides data support for frost damage mitigation and stability assessment of canals in cold regions.

Keywords: cold region; freeze–thaw action; canal slope; stability; numerical analysis

Academic Editor: Chin H Wu

Received: 13 February 2026
Revised: 12 March 2026
Accepted: 17 March 2026
Published: 19 March 2026

1. Introduction

Freeze–thaw cycles are recognized as a significant weathering process that frequently occurs in cold regions, and the number of these cycles can exceed hundreds per year in northeastern and northwestern China [1,2], as shown in Figure 1a. Under the effect of freeze–thaw cycles, a fracture network is formed in the rock and soil mass, which consequently induces a significant loss of its mechanical strength, including tensile strength and fracture toughness [3,4]. Statistics indicate that the total length of canals in China exceeds 4.5×10^6 km, with over 60% of them located in cold regions [5]. Severe frost damage to canals has existed in 13 provinces across China [6]. As air temperatures decrease, moisture migration within the soil leads to significant frost heave deformation in slopes [7,8].

This deformation is further intensified when slope foundations are in direct contact with water. The damage induced by freeze–thaw action, including slope failure, lining board cracking and uplift, reduced the service life and performance of canals, as shown in Figure 1b–d. According to the standard code for rational service life and durability design of water resources and hydropower projects (SL654-2014) [9], the reasonable service life of irrigation canals is at least 20 years. During this period, canal slopes are subjected to cyclic freeze–thaw action, whereby the cumulative damage leads to a progressive deterioration of the soil and, ultimately, triggers slope failure.

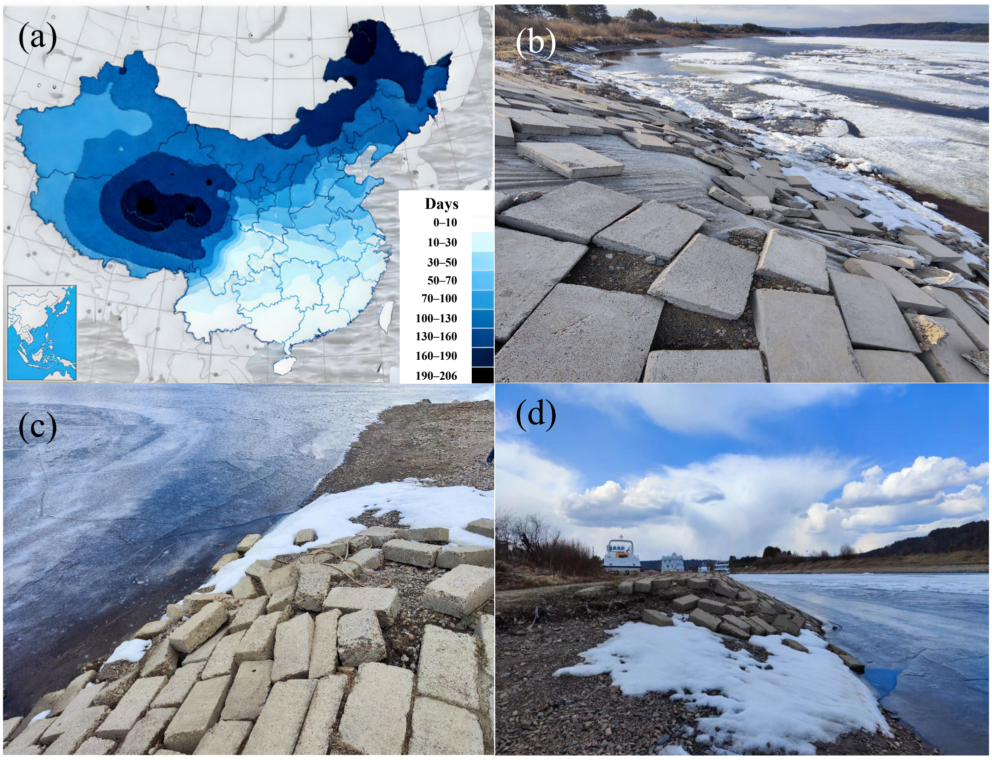

Figure 1. Pictures of canal damages in the northeast of China. (**a**) distribution of freeze-thaw cycles; (**b**) lining board cracking; (**c**) lining board cracking and uplift; (**d**) slope failure.

Numerous instances of damage have been attributed to the coupled effects of water, heat, and mechanical stress [10–12]. Temperature fluctuations directly govern the phase change of water, which generates cyclic stresses and alters soil hydraulic properties such as permeability [13]. This in turn increases pore pressure and reduces soil shear strength, thereby accelerating slope failure. More importantly, the designed service life of canals spans several decades, which markedly increases the vulnerability to damage under freeze–thaw action. Therefore, the investigation onto the thermo-hydro-mechanical (THM) conditions of canals in the long term can not only help us reveal the evolution mechanism of freeze–thaw damage but also provide a reference for the anti-freezing design measures.

Until now, many scholars have focused on the THM conditions of canal slopes during freeze–thaw action based on in situ monitoring, model tests, and numerical analysis. In terms of in situ monitoring, Wu et al. revealed the temperature and accumulated water content variation process at the top and middle of both shady and sunny slopes, and further compared the temperature variation, frozen depth and deformation in different sections [14]. Ge et al. found that the canal slope with a two-layer composite geomembrane lining structure can increase the soil temperature by 7%, thereby reducing the deformation magnitude by 38% [15]. Chen et al. analyzed the temperature and pore water pressure of a canal, and further proposed and compared several anti-freezing measures from the perspectives of economy and reliability [16]. As a research method that comprehensively reflects the actual conditions of canals, in situ monitoring not only provides reliable boundary conditions for model tests and numerical simulations but also serves as a benchmark for verifying the reliability of their results. In contrast, model tests and numerical simulations are widely adopted due to their advantages in reducing test time and costs compared with in situ monitoring [17–19]. On the basis of model tests, Li et al. found that moisture significantly accumulates at the freezing front under thermal gradients. In particular, deformation at the slope toe tends to be more pronounced than in other areas [20]. Through field measurements of temperature, water content, and frost heave deformation on two canal slopes with different protective layers, Jiang et al. demonstrated that polyester geotextiles outperform composite geomembranes in terms of performance [21]. Wang et al. found that, as the temperature of the slope decreases, the maximum deformation occurs at 1/2 of the height of the canal, and that there is significant residual deformation on the slope surface after thawing [22]. Jiang et al. found that under an ambient temperature of -15 °C and a radiation intensity difference of 39.2 W/m^2, the shady slope exhibits a frozen depth and deformation approximately 1.4 times greater than those of the sunny slope [23]. Based on numerical analysis, Li et al. examined the temperature and deformation of an earth-rock dam slope, revealing that the freeze–thaw influence depth is approximately 2 m, and that frost heave deformation due to water migration ranges from 20 cm to 30 cm. The frost heave deformation of the slope caused by water migration ranges from 20 cm to 30 cm [24]. Wang et al. proposed a mechanical model for trapezoidal canals lined with double-layer geomembranes and elucidated the reinforcement effects of this lining system under freeze–thaw conditions. They also calculated the variations in internal stress of different types of canals in a full freeze–thaw process [25]. Li et al. evaluated the temperature distribution, moisture migration, and deformation characteristics of a conventional canal and an improved lining structure composed of concrete slabs, polystyrene insulation, sandy gravel, and a composite geomembrane. Their findings confirmed that the new canal lining structure is more suitable for canals in cold regions [26].

In addition, some research on the long-term stability and safety performance of slopes in cold regions under freeze–thaw cycles have been conducted. McRoberts and Morgenstern [27] classified the instability modes of frozen soil slopes into three categories, including the mudflow type, slip type, and collapse type. Zheng and Chao [28] found that the slope exhibits peak instability risk in the freeze–thaw phase transition period through numerical simulation. Specifically, during the initial freezing stage, insufficient ice crystal bonding leads to an accumulation of displacement. Subsequently, the sharp drop in bonding strength during melting further exacerbates structural weakening. Li and Yu [29] developed a multifield coupled model for slopes in cold regions and quantified the evolution law of safety factors during temperature alternation using the strength reduction method, revealing the inherent relationship between stress redistribution and displacement field evolution. Li [30] utilized the strength reduction method to evaluate the safety factors of slopes under various moisture contents and freeze–thaw cycles considering the thermo–hydro coupling effect. The results revealed that the safety factor declined gradually with an increasing number of freeze–thaw cycles, eventually stabilizing at a lower level.

While various anti-freezing measures have been proposed based on the aforementioned research, slope failures induced by freeze–thaw action remain frequent, particularly during the spring thawing period. Currently, there is a lack of comprehensive research on the correlation between the evolution of THM characteristics and the long-term stability of canal slopes. To fill these gaps, this study conducted a series of model tests and numerical simulations to reveal their change behaviors and determine the critical state of the slope in service. This study can provide a scientific basis and reference for the stability assessment and frost damage prevention of canal slopes in cold regions.

2. Experimental Designs

2.1. Basic Information of the Canal Slope

The North Nenjiang River Diversion Canal is situated in Heilongjiang Province, northeastern China. The main canal extends 202 km in total, with an additional 40 km of branch canals. The annual flow is 4.65 × 10 m^3. The project area is situated within the geographical coordinates of 124° E–126° E and 46° N–48° N. Soil samples were collected at a depth ranging from 1.5 to 2.5 m. The properties of the soil were measured in accordance with the Geotechnical Test Methods Standard [31], and the soil was classified as low-plasticity clay (CL). The main properties of the tested soil are shown in Table 1.

Table 1. The properties of tested soil.

Parameters			Unit	
Particle composition	Sand	0.5–0.25 mm	%	0.4
		0.25–0.075 mm	%	1.3
	Silt	0.075–0.005 mm	%	66.1
	Clay	<0.005 mm	%	32.2
Dry density			g/cm^3	1.55
Specific gravity				2.70
Porosity ratio			%	0.8
Liquid limit			%	35.6
Plastic limit			%	23
Classification				CL

2.2. Experimental Procedure

Considering that there are no external loads on canal slopes under natural conditions, the slope model is only required to satisfy the similarity principles governing the time scale and geometric scale. Based on previous literature, the correlation between the geometric scale and time scale is expressed as follows [32]:

$$c_t = c_l^2 \tag{1}$$

where c_t and c_l denote time scale and geometric scale, respectively.

Considering the actual laboratory dimensions, the c_l is set as 1:15. Then, the c_t is calculated as 1:225. Further, the duration for each stage of the experiment is listed in Table 1. Then, the actual air temperature at the study site can be simplified as a linear variation which includes two cooling stages, a constant negative temperature stage, a warming stage, and a constant positive temperature stage, as shown in Figure 2. The temperature range and duration at each stage are listed in Table 2.

Figure 3a shows the profile of the model slope. The heights of the slope top and the slope toe are 0.5 m and 0.2 m, respectively. The horizontal length of the slope surface is 0.8 m. The temperature was monitored by thermistor temperature sensors with a precision of ±0.02 °C and recorded by a CR1000 data collector (Campbell Scientific, Inc., Logan, UT, USA). The data collection was performed at 5 min intervals. The temperatures at two different sections, namely T1 and T2, were recorded during the freeze–thaw process. According to previous research, the maximum frozen depth under extreme conditions in the North Nenjiang River diversion canal area of Heilongjiang Province can reach 2.9 m [33]. The geometric scale is 1:15, and so the corresponding maximum frozen depth in the model test is 19.3 cm. The vertical depths of the sensors were 2 cm, 4 cm, 6 cm, 8 cm, 10 cm, 12 cm, 16 cm, and 20 cm, respectively.

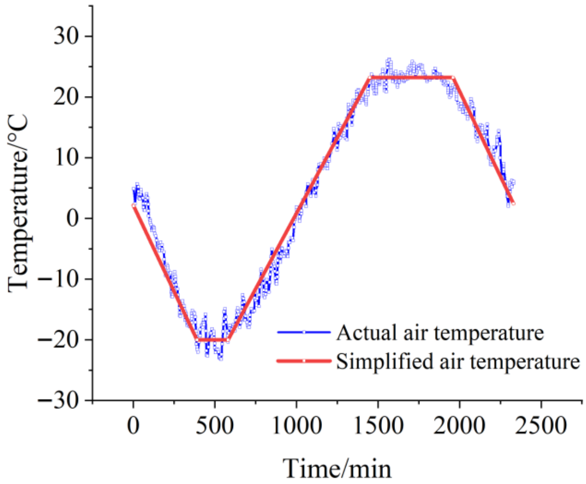

Figure 2. Comparison of air temperature before and after simplification.

Table 2. Air temperature variation process in experiment.

Temperature Control Stage	Duration/h	Temperature Range/°C
Cooling process	6.29	2~−20.0
Constant negative temperature stage	3.2	−20
Warming process	14.4	−20~23.3
Constant positive temperature stage	8.64	23.3
Cooling process	6.4	23.3~2.0

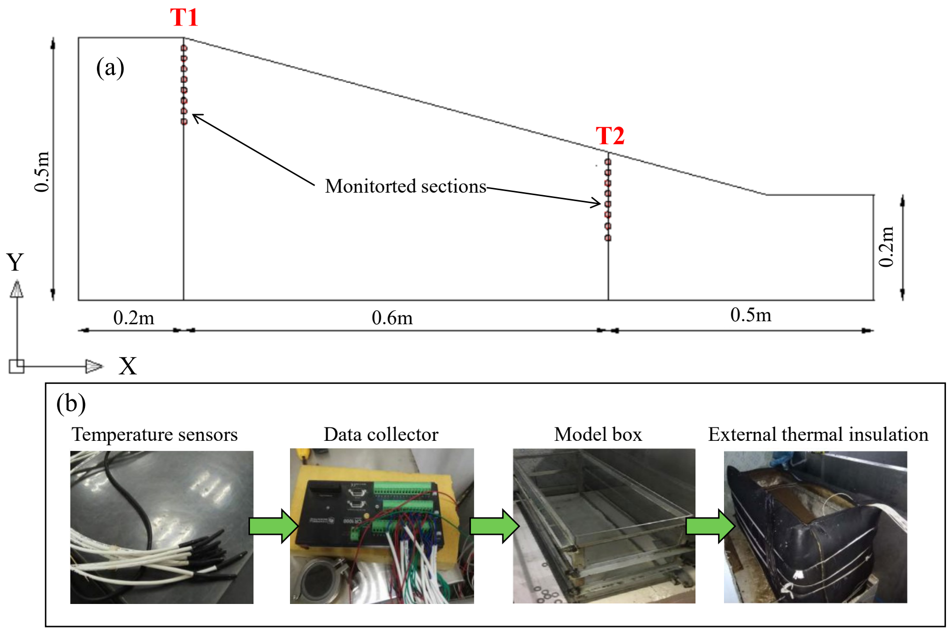

Figure 3. Model construction and monitoring point layout. (**a**) the profile of the model slope; (**b**) the process of arranging sensors.

The model slope was filled in an organic glass box with dimensions of 1.3 m × 0.5 m × 0.5 m (length, width, and height). The glass box was fixed with angle steel on all sides to prevent frost heave damage. In addition, the model slope was surrounded by insulation materials with a thickness of 10 cm to reduce the heat exchange between its lateral walls and the external environment, as shown in Figure 3b. The collected soil was oven-dried, pulverized, and mixed with a predetermined amount of water. The mixture was then sealed for 48 h to ensure uniform water distribution before being used for the model slope. The model slope was filled in 10 layers vertically. The required mass of soil for each layer was calculated according to the volume, dry density, and water content. The uniformity of the soil was ensured by controlling the compaction frequency and the thickness of each soil layer. To ensure structural integrity between layers, the surface of each compacted layer was roughened before filling the next layer.

2.3. Numerical Model

2.3.1. Governing Equations

The governing equation for the temperature field can be defined as [34]:

$$\rho c_p \frac{\partial T}{\partial t} = \lambda \nabla^2 T + L\rho_i \frac{\partial \theta_i}{\partial t} \tag{2}$$

where ρ is the soil density; ρ_i denotes the density of ice; c_p represents the equivalent volumetric heat capacity; T is temperature; λ is the thermal conductivity; ∇ is the differential operator.

The heat capacity under thawed and frozen states can be expressed as follows:

$$C_u = C_{du}\rho_u \tag{3}$$

$$C_f = C_{df}\rho_f \tag{4}$$

where C_u is the volumetric heat capacity of thawed soil; C_f is the volumetric heat capacity of frozen soil. C_{du} and C_{df} are the specific heat capacities of thawed and frozen soil, respectively. ρ_u and ρ_f are the natural densities of thawed soil and frozen soil, respectively.

C_{df} can be expressed as [35]:

$$C_{df} = \frac{C_{af} + (\theta - \theta_u)C_i + \theta_u C_w}{1 + \theta} \tag{5}$$

where the C_{af}, C_i, and C_w are the specific heat capacities of the frozen soil skeleton, ice, and water; θ is the total water content; θ_u is the unfrozen water content.

The thermal conductivity of soil can be defined as [35]:

$$\lambda = \theta_u \lambda_u + \theta_i \lambda_i + (1 - \theta_s)\lambda_s \tag{6}$$

where λ_u, λ_i, and λ_s are the thermal conductivities of water, ice, and soil grains, respectively.

The governing equation for the water field can be expressed as:

$$\frac{\partial \theta_u}{\partial t} + \frac{\rho_i}{\rho_w}\frac{\partial \theta_i}{\partial t} = \nabla[D(\theta_u)\nabla\theta_u + k(\theta_u)] \tag{7}$$

where $D(\theta_u)$ is the hydraulic diffusion coefficient.

$D(\theta_u)$ can be calculated as [36,37]:

$$D(\theta_u) = \frac{k(\theta_u)}{C(\theta_u)} I \tag{8}$$

$$I = 10^{-10\theta_i} \tag{9}$$

$$C(\theta_u) = \frac{a_0 m}{(1-m)(\theta_s - \theta_r)} S^{1/m}\left(1 - S^{1/m}\right)^m \tag{10}$$

where $k(\theta_u)$ is the permeability of soil; $C(\theta_u)$ is the specific water capacity; I is the impedance coefficient of ice; θ_r is the residual water content; θ_s is the saturated water content; a_0 and m are the empirical parameters, respectively.

The permeability of soil can be expressed as [38]:

$$k(\theta_u) = k_s k_r I \tag{11}$$

$$k_r = S^{l/2}\left[1 - \left(1 - S^{1/m}\right)^m\right]^2 \tag{12}$$

where k_s denotes the permeability coefficient of saturated soil; k_r represents the relative permeability coefficient; l is the empirical parameter.

To solve the governing equation, the relationship between ice content and unfrozen water content is defined as [39]:

$$B_f = \frac{\theta_i}{\theta_u} = \begin{cases} 1.1\left(\frac{T}{T_f}\right)^B - 1 & T < T_f \\ 0 & T \geq T_f \end{cases} \tag{13}$$

where T_f is the initial freezing temperature of the soil; B is the empirical parameter.

During the freeze–thaw process, the stress redistribution caused by external loads, water pressure, and ice pressure is neglected. The stress caused by in situ frost heave and ice segregation heave is considered. The soil can be recognized as an elastic body that is governed by equilibrium, geometric, and constitutive equations, which can be expressed as:

$$[A][\sigma] = [F] \tag{14}$$

$$\left[A^T\right][d] = [\varepsilon] - [\varepsilon_0] \tag{15}$$

$$[D][\varepsilon] = [\sigma] \tag{16}$$

where $[A]$ is the differential operator; $[\sigma]$ is the stress tensor; $[F]$ is the force vector; $[d]$ is the displacement vector; $[D]$ is the elastic matrix; $[\varepsilon]$ is the strain; $[\varepsilon_0]$ is the initial strain, which can be expressed as:

$$[\varepsilon_0] = \frac{1}{3}[\varepsilon_v, \varepsilon_v, \varepsilon_v, 0, 0, 0]^T \tag{17}$$

ε_v can be further calculated as:

$$\varepsilon_v + 0.09(\theta_0 + \Delta\theta - \theta_u) + \Delta\theta - n + 3\alpha_s\theta_s\left(T - T_f\right) + 3\alpha_w\theta_u\left(T - T_f\right) + 3\alpha_i\theta_i\left(T - T_f\right) \tag{18}$$

where $\Delta\theta$ is the volumetric water content of migrated water; α_s is the expansion coefficient of soil; α_w is the expansion coefficient of water; α_i is the expansion coefficient of ice; n is the porosity; T_f is the phase transition temperature.

The elastic modulus of the soil changes continuously, accompanied by the ice-water phase transition. The relationship between the elastic modulus and temperature can be described as follows [40]:

$$E = \begin{cases} (a_1 + b_1 T)^{0.6} & T \leq T_\mathrm{f} \\ E_0 & T > T_\mathrm{f} \end{cases} \tag{19}$$

where E is the elastic modulus; a_1 and b_1 are empirical parameters that are related to soil properties.

2.3.2. Boundaries and Parameters

The air temperature at the slope surface is controlled in accordance with Table 2, with a convective heat transfer coefficient of 15 W/(m^2·°C). The lateral boundaries are adiabatic and impermeable. In the stress field, the slope surface and bottom wall are set as a free and a fixed boundary, respectively. Roller support boundaries are applied to the lateral boundaries of the slope. According to the monitoring data, the initial temperature from the slope surface to the slope bottom ranges from 6 °C to 4 °C. The initial volumetric water content was set at 22%. A total of 2924 triangular elements were generated in the geometric model.

The stability of the canal slope was evaluated using the strength reduction method. This method reduces the shear strength parameters of the slope soil until the slope reaches a critical stability state. The formula for reducing the strength parameters can be expressed as:

$$c' = c/F_s \tag{20}$$

$$\varphi' = \arctan(tan\ \varphi/F_s) \tag{21}$$

where c is the cohesion of soil under the actual shear strength; φ is the internal friction angle of soil; c' is the cohesion of soil after shear strength reduction; φ' is the internal friction angle after shear strength reduction; F_s is the safety factor.

Based on studies conducted on the same soil type and within the same research region, the correlation between soil cohesion, internal friction angle, number of freeze–thaw cycles, and unfrozen water content is given by [41]:

$$c(n,w) = 59.08e^{-0.07822x-4.35101w} \tag{22}$$

$$\varphi(n,w) = 59.85e^{-0.02398x-6.69701w} \tag{23}$$

where x denotes the number of freeze–thaw cycles; w represents the unfrozen water content.

The required parameters of the numerical model are listed in Table 3.

Table 3. Values and units of the required parameters.

Symbol	Value	Unit	Symbol	Value	Unit
C_s	800	J/(kg·K)	a_1	5×10^6	Pa
C_i	2100	J/(kg·K)	b_1	2×10^6	Pa/K
C_w	4200	J/(kg·K)	ν	0.3	/
λ_i	2.2	W/(m·K)	l	0.5	/
λ_w	0.6	W/(m·K)	m	0.4	/
ρ_s	1750	kg/m^3	a	3	1/m
ρ_w	1000	kg/m^3	a_s	1×10^{-5}	1/K
ρ_i	900	kg/m^3	a_w	2.1×10^{-4}	1/K
θ_s	29	%	a_i	5×10^{-5}	1/K
θ_r	0.2	%	B	0.56	
T_f	−0.24	°C	k_s	1×10^{-6}	m/s

3. Results and Analysis

3.1. Monitored Temperature and Model Validation

The temperatures in the T1 section and the T2 section are shown in Figure 4. Soil temperatures decrease with increasing depth during the freezing process, while they increase with increasing depth during the warming process. The coldest temperatures at different depths in the T1 section are −4.68 °C (2 cm), −4.18 °C (4 cm), −2.45 °C (6 cm), −1.52 °C (8 cm), −0.72 °C (10 cm), −0.42 °C (12 cm), −0.12 °C (14 cm), and 0.32 °C (16 cm), respectively. However, the values for the T2 section are −3.79 °C (2 cm), −2.90 °C (4 cm), −2.70 °C (6 cm), −1.61 °C (8 cm), −0.55 °C (10 cm), −0.29 °C (12 cm), 0.21 °C (14 cm), and 0.01 °C (16 cm), respectively. The warmest temperatures in the T1 section and T2 section are also different. Taking the temperatures at a depth of 2 cm as an example, the warmest temperatures are 21.08 °C and 18.53 °C in the T1 section and T2 section, respectively. Therefore, it is clear that the variation ranges at the same depths in the T1 section are larger than those of the T2 section. This discrepancy arises because the T1 section is slightly more elevated than the T2 section, making it more responsive to fluctuations in air temperature.

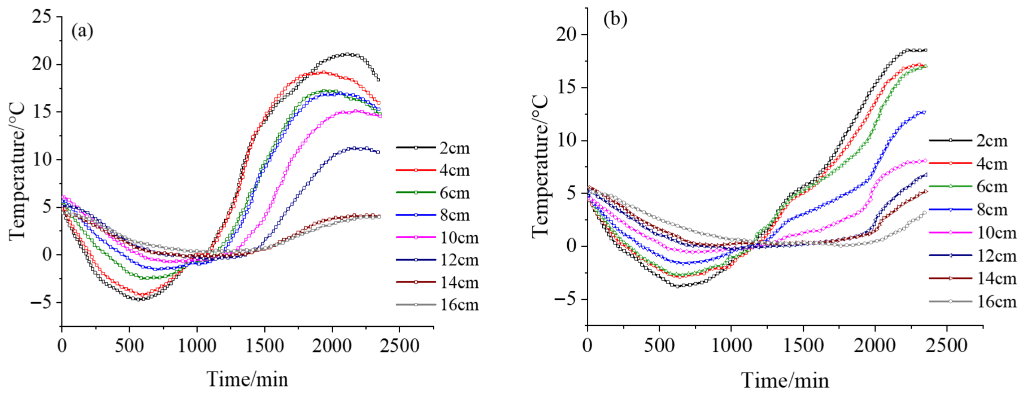

Figure 4. The temperature variation at different depths in monitored section. (**a**) T1 section; (**b**) T2 section.

In this research, the mean bias error (*MBE*) is utilized to assess the discrepancies between simulated and measured values. A lower *MBE* value signifies higher model accuracy. The formula for *MBE* is defined as:

$$MBE = (1/n)\sum_{i=1}^{n} \frac{|M_i - E_i|}{E_i} \tag{24}$$

where the M_i is the numerical results; E_i is the measured results; n is the total amount of data.

The measured and simulated temperatures at 190 min and 810 min in the T2 section are depicted in Figure 5. It can be seen that the simulated values are in good agreement with the measured values. With *MBE* values of 0.35 and 2.25 at the two respective time points, the numerical model exhibits reliable accuracy.

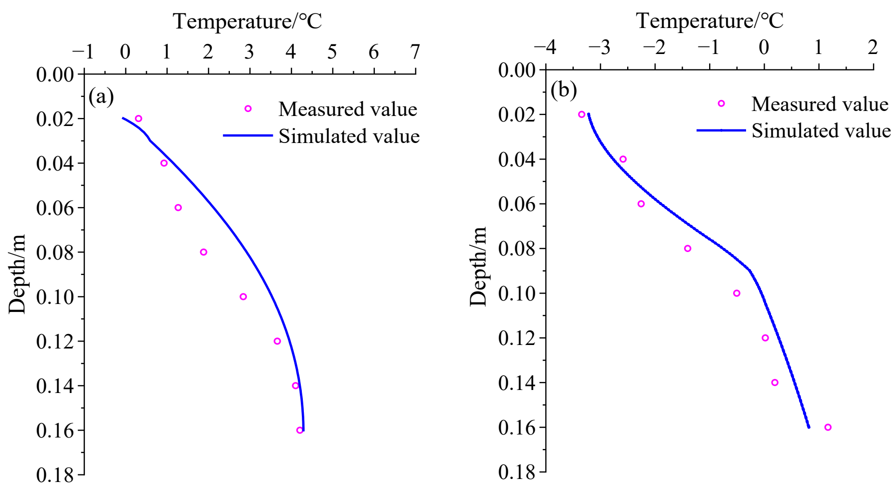

Figure 5. Comparison between measured data and simulated data. (**a**): 190th min; (**b**): 810th min.

3.2. Evolution Process of Hydrothermal Characteristics

The simulated temperature fields of the slope at years 3, 8, 14, and 20 are shown in Figure 6. The maximum frozen depth of the slope reflects the potential damage zone, which is also outlined in the figure. In general, the temperatures from slope surface to slope bottom range from −8 °C to 4 °C. Meanwhile, the isotherms are distributed parallel to the slope surface. However, the maximum frozen depth increases significantly as the service time extends. In the 3rd year, the maximum frozen depth reaches 0.081 m, with the frozen zone primarily concentrated near the slope surface. By the 8th year, the maximum frozen depth increases to 0.082 m. As the operation time extends to the 14th year and 20th year, the maximum frozen depth increases to 0.090 m and 0.098 m, respectively. The annual average growth rate of the maximum frozen depth from the 3rd year to the 14th year is relatively high. In addition, since the geometric scale is 1:15, the actual maximum frozen depths correspond to 1.21 m, 1.23 m, 1.35 m, and 1.47 m in the 3rd year, 8th year, 14th year, and 20th year, respectively. This trend can be attributed to the fact that, following slope construction, temperatures from the slope surface to the bottom are always positive. At this time, the temperatures inside the slope are not stable, and the cold energy introduced into the slope in winter can quickly drive the freezing front downward. As the number of freeze–thaw cycles increases, the internal temperature field of the slope gradually stabilizes under the influence of ambient air temperatures.

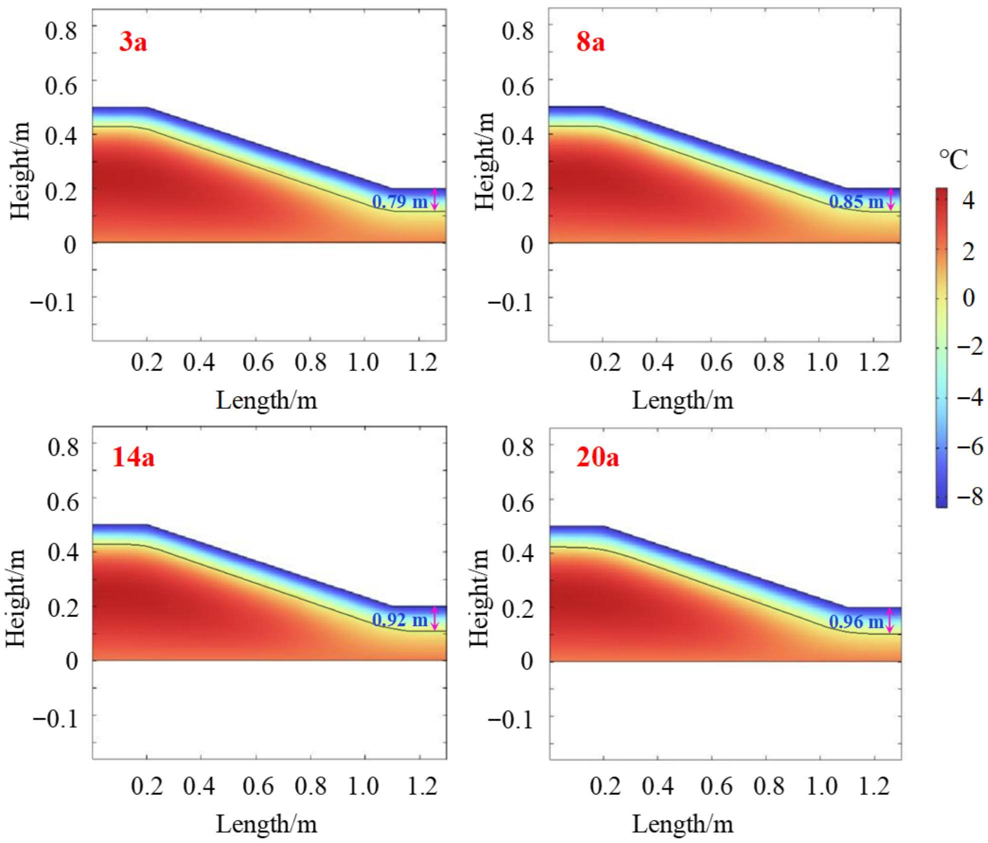

Figure 6. Temperature distribution during different service times.

However, the migration of water from the unfrozen areas to the frozen areas during the freezing process increases the thermal conductivity of the soil in the upper part of the slope. This allows cold energy to transfer downward more effectively in winter and further increases the maximum frozen depth. Therefore, from the perspective of controlling the temperature of cold-region canal slopes, it is necessary to install a thermal insulation layer of a specific thickness on the slope surface to prevent the frozen depth from extending continuously downward and to elevate the temperature of the slope in winter after construction.

Figure 7 illustrates the distribution of unfrozen water content within the canal slope during its 3rd, 8th, 14th, and 20th years of operation. Due to freezing, the unfrozen water content is lowest near the slope surface and gradually increases with depth. A decreasing trend is observed in the maximum unfrozen water content over time, with values of 0.2 (3rd year), 0.18 (8th year), 0.16 (14th year), and 0.14 (20th year), respectively. Therefore, it indicates that frost damage to the canal becomes progressively more severe during its service life, which is consistent with the thermal evolution described previously.

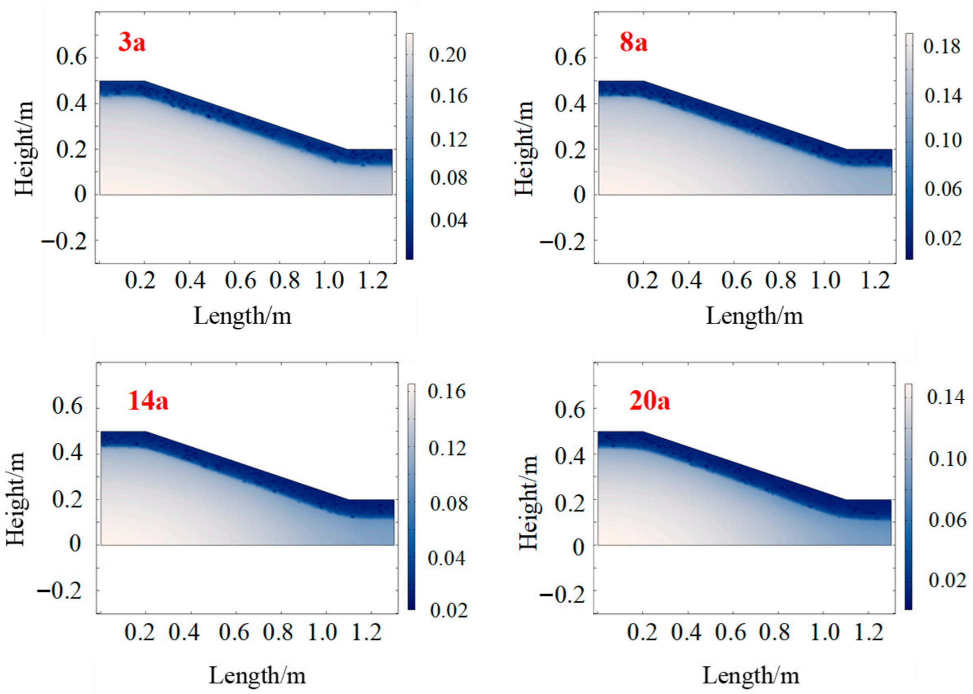

Figure 7. Unfrozen water content distribution during different service times.

3.3. Evolution Process of Deformation

Slope failures are closely related to slope deformation during freeze–thaw cycles. The deformations at 1/2 and 1/3 of the slope's height are shown in Figure 8. It can be observed that the deformations of the slope show a sustained growth trend with the number of freeze–thaw cycles. The deformation growth rate exhibits an initial rapid phase followed by gradual deceleration. The maximum deformations occurring at the 1/2 slope height are notably greater than those at the 1/3 slope height, which agrees well with the previous literature and actual damage conditions of the slope [42,43]. The maximum deformations are 4.5 mm (1/2 slope height) and 4.0 mm (1/3 slope height), respectively. This is because the 1/3 slope height is close to the slope toe, which provides a restraint against frost heave. Additionally, the overburden pressure of the upper soil restricts deformation at this location. In contrast, the 1/2 slope height acts as a free deformation zone, consequently leading to more significant displacement. Damage, such as overlapping and cracking of the lining boards, is more likely to occur at this position. To alleviate this issue, some measures such as replacing the slope soil or enhancing compaction during filling should be implemented in construction.

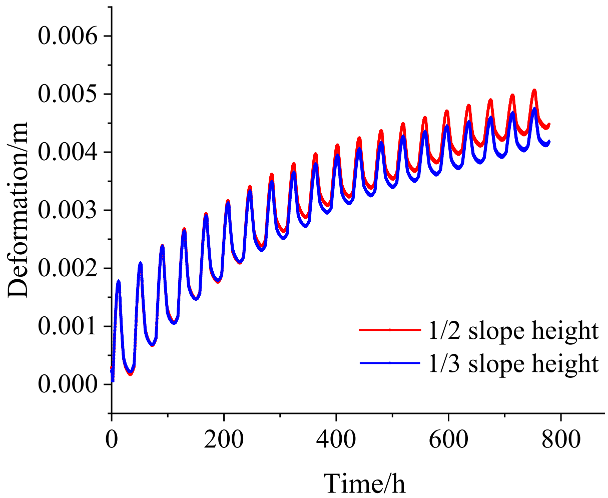

Figure 8. Deformations of slope surface.

3.4. Evolution Process of Stability

To analyze the stability of the canal slope, a full-scale canal slope model was established based on the geometric scale. Considering that slope failures often occur during the spring thawing period, the slope deformations in Aprils of different service years were selected as an example for analysis, as shown in Figures 9 and 10. Regardless of the service time of the canal, the plastic strains were concentrated at the slope toe. As the service time increases, the safety factors decrease significantly. The correlation between the safety factor and freeze–thaw cycles count can be described by an exponential function. Moreover, at years 3, 8, 14, and 20, the safety factors are 2.19, 1.86, 1.49, and 1.18, respectively. Compared with that of the first year, the safety factor decreased by 1.27 after 20 freeze–thaw cycles. It is evident that freeze–thaw cycles can accelerate slope failure. This is primarily attributed to the deterioration of both cohesion and the internal friction angle of the slope soil under freeze–thaw action. Therefore, it is essential to carry out reinforcement measures for the slope toe in cold regions. If no corresponding measures are taken during construction, it is recommended to set up temporary reinforcement measures during the spring thawing period to prevent slope instability.

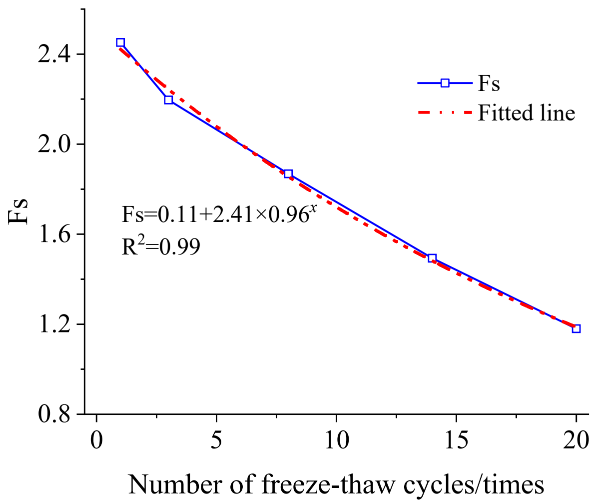

Figure 9. Relationship between safety and number of freeze–thaw cycles.

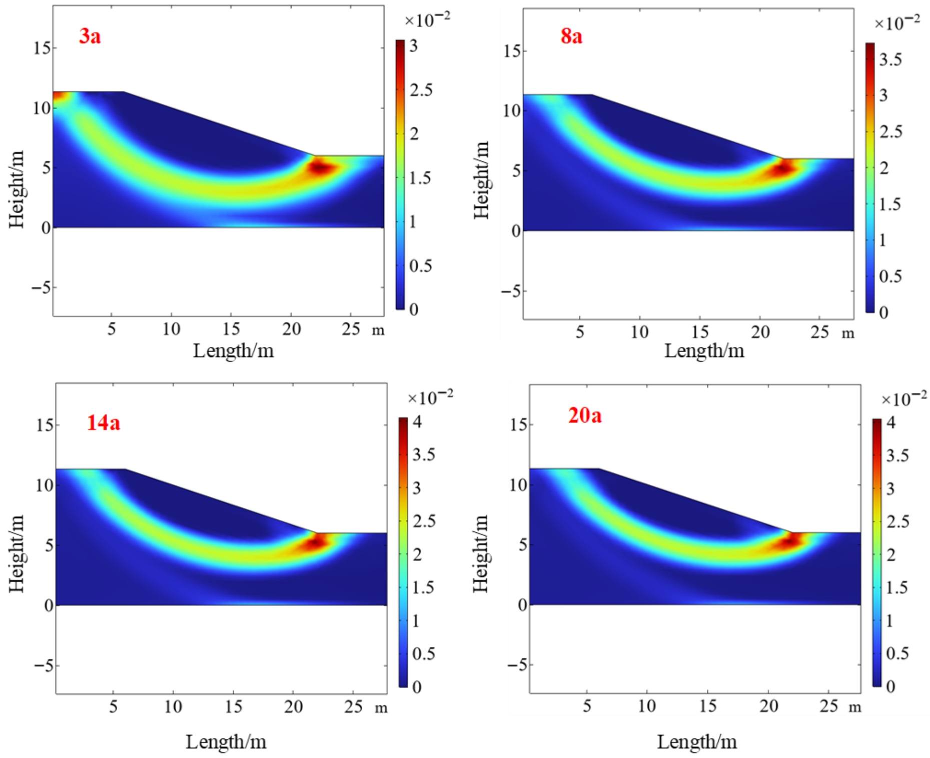

Figure 10. Displacement distribution of slope in April (unit: m).

4. Discussions

Slope stability is governed by a multitude of factors, including soil properties [44], hydrogeological conditions [45,46], and external environmental disturbances [47]. Among them, the presence of freeze–thaw cycles triggers the coupled water-heat-deformation evolution of the slopes [48,49]. As a result, the physical-mechanical characteristics and internal structural balance of the soil are disrupted, ultimately leading to the instability of canal slopes [50,51]. From a microscopic perspective, freeze–thaw cycles impose significant alterations on the internal microstructure of soils [52,53]. The phase transition of pore water into ice facilitates the rearrangement of soil particles, which further promotes the expansion of inter-aggregate pores and the initiation and propagation of microcracks. This process destroys the original cementation bonds between particles, loosens the soil skeleton, and increases porosity. With a continued increase in the number of cycles, these microstructural changes become irreversible, progressively degrading the soil's cohesion and shear strength. As the temperature decreases, cryogenic suction and ice pressure within the slope increase, and unfrozen water migration further intensifies frost heave. The maximum deformation is concentrated in the middle of the slope. As temperature rises, the slope surface begins to thaw, and frost heave disappears. However, due to the accumulation of residual deformation, the deformation cannot be fully restored [21]. With an increasing number of freeze–thaw cycles, the frost depth increases and unfrozen water content decreases remarkably. Meanwhile, the residual deformation accumulates continuously. These progressive changes act synergistically and ultimately trigger the slope instability. In addition, due to sudden change in slope geometry and significant shear stress concentration at the slope toe, it easily yields first and forms the plastic deformation zone [54]. Moreover, freeze–thaw cycles deteriorate the mechanical properties of the soil at the slope toe, thereby exacerbating structural instability [55]. Therefore, the plastic deformation zone typically initiates at the slope toe, progressively extends upward toward the crest, and ultimately develops into a continuous sliding surface.

The stability of the canal slope is significantly affected by temperature fluctuations. Taking the canal in the 20th year of service as an example, the safety factor is shown in Figure 11. It is evident that the safety factor of the canal slope continues to rise as a result of ice cementation. The safety factors in November, December, January and February are 1.07, 1.14, 1.19 and 1.21, respectively. The maximum safety factor occurs in March of the following year, with a value of about 1.22. Compared with November of the previous year, the safety factor increased by 0.15. As the temperature rises, the safety factor rapidly decreases due to the loss of ice cementation after March. As shown in Figures 10 and 11, the safety factors for March and April are 1.22 and 1.18, respectively. In addition, the instability of the canal slope often initiates at the slope toe. Subsequently, as shear strength decreases, the plastic failure zone develops towards the slope top. Therefore, it is essential to enhance the monitoring of slope deformation during March and April. Some temporary reinforcement measures such as stacking sandbags and installing shallow anchor rods should be implemented if necessary.

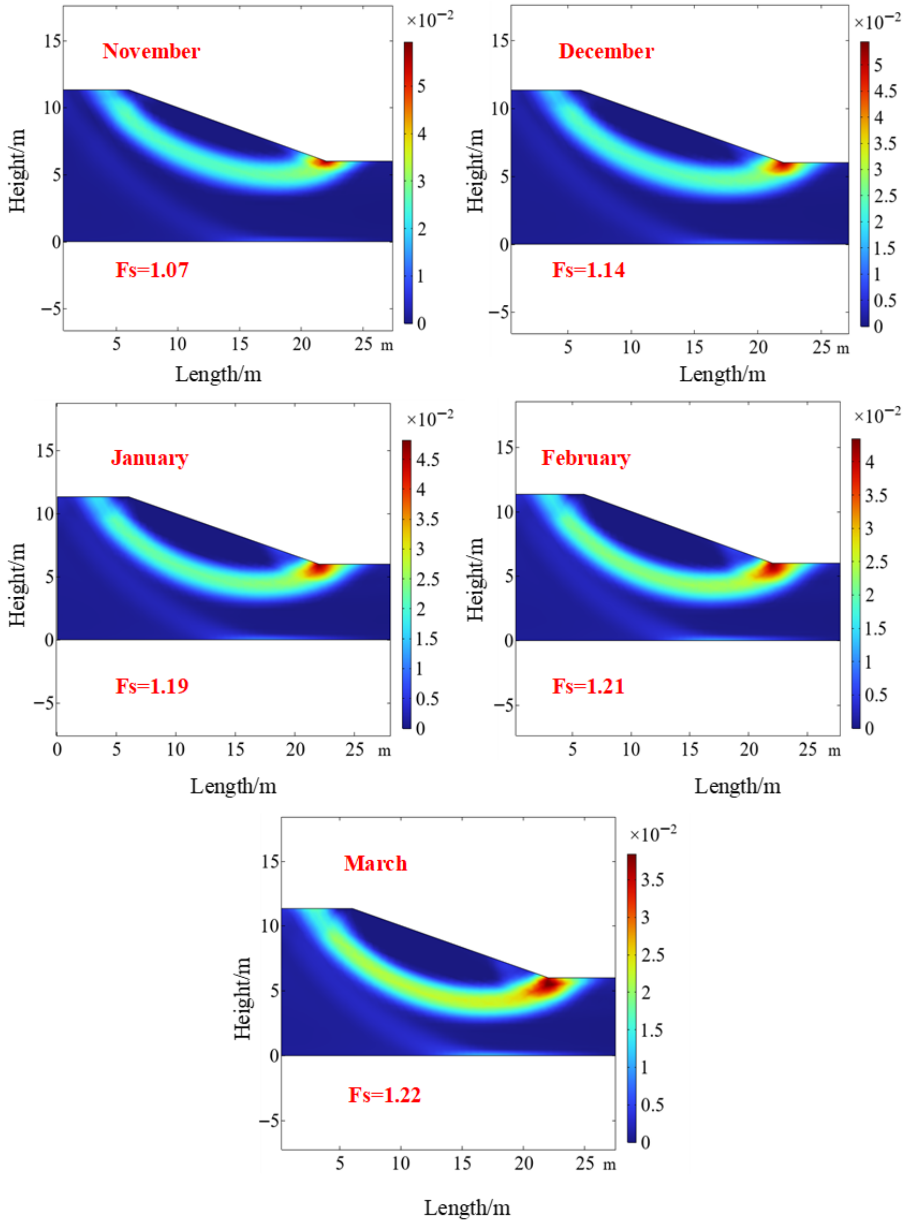

Figure 11. Displacement distribution of slope in different months (unit: m).

Although this study focuses on the problem of slope instability caused by variations in hydro-thermal-mechanical characteristics under freeze–thaw action and has achieved certain results, it still has some limitations due to the constraints of test conditions and research methods. First, the experiments in this study are carried out based on model tests, which inevitably differ from the actual service environment of canal slopes, such as the influences of rainfall and snowfall. In the future, we will continue to improve the model test conditions to fill the gaps between model tests and actual engineering. Second, the THM coupling model established in this study does not incorporate the influence of slope soil creep on stability. In practice, slope failure in cold regions is often a progressive process caused by the combined action of cumulative long-term freeze–thaw effects and creep deformation. In future research, a hydro-thermal-mechanical numerical model that accounts for the creep characteristics of the soil will be developed.

5. Conclusions

In this study, the THM behavior of a canal slope was investigated through a combination of model testing and numerical simulation. The evolution of temperature distribution, maximum frozen depth, unfrozen water content, and deformation during service periods was revealed. The safety factor at the critical state of the slope was calculated. The main findings are summarized as follows:

(1) The temperature inside the canal slope is significantly affected by the ambient air temperature. In the warm season, the temperature decreases with increasing depth, whereas temperature variation shows the opposite trend during the cold season. In addition, due to the larger variation range at the same depth in the T1 section than in the T2 section, the temperature gradient gradually decreases with increasing slope depth.

(2) Within the 20 years after the slope was constructed, both maximum frozen depth and the frost heave deformation exhibit a continuous increase. The development of the maximum frozen depth is relatively rapid during the first 14 years. The maximum deformation appears in the middle of the slope, with a value of 5.0 mm in the cold season. In addition, the unfrozen water content also decreases with service time. The maximum unfrozen water content inside the slope decreases by 0.06 from the 3rd year to the 20th year.

(3) During the long-term service of the canal slope, its stability gradually decreases due to freeze–thaw action. Slope failure initiates with the sliding of the slope toe. The evolution of the canal slope safety factor is not only dependent on the service time but also shows obvious seasonal fluctuations. Affected by the air temperature, the safety factor increases significantly from November to March of the following year due to freezing. Subsequently, the gradual thawing of the soil after March leads to a decrease in the safety factor. Therefore, special attention should be paid to the canals in cold regions during the spring thaw period.

Author Contributions: L.Q.: Formal analysis, Writing—review and editing. Y.M.: Methodology, Writing—review and editing. H.S.: Resources, Supervision, Writing—review and editing. C.S.: Resources, Writing—review and editing, Funding acquisition. H.J.: Funding acquisition, Writing—review and editing. Y.P.: Resources, Validation. W.J.: Writing—review and editing. All authors have read and agreed to the published version of the manuscript.

Funding: This work was supported by the Natural Science Foundation of Jiangsu Province (BK20250406), Research on the Intelligent Scheduling Platform System for Smart Irrigation Districts (CDY-2024017-KJ03) and Natural Science Foundation of Heilongjiang Province (ZD2023E007).

Data Availability Statement: The original contributions presented in this study are included in the article. Further inquiries can be directed to the corresponding authors.

Conflicts of Interest: Author Hongbo Sun was employed by the company Heilongjiang Dingjie Road and Bridge Engineering Co., Ltd. Author Changhong Song was employed by the company Heilongjiang Water Resources Investment Group. Author Wanying Jin was employed by the company Beijing Zhongshui Lide Technology Development Co., Ltd. (Shandong Branch). The remaining authors declare that the research was conducted in the absence of any commercial or financial relationships that could be construed as a potential conflict of interest.

References

1. Wu, H.; Jin, H.; Yan, Y.; Xia, J. Environmental zonation and life prediction of concrete in frost environments. *J. Zhejiang Univ. (Eng. Sci.)* **2012**, *46*, 650–657.
2. Niu, F.; Jiang, H.; Su, W.; Jiang, W.; He, J. Performance degradation of polymer material under freeze-thaw cycles: A case study of extruded polystyrene board. *Polym. Test.* **2021**, *96*, 107067. [CrossRef]
3. Wang, L.; Xue, Y.; Zhu, L.; Cao, X.; Li, X.; Ranjith, P.G. Fracture evolution of granite under cyclic thermal shocks: Effects of liquid nitrogen cooling on strength, toughness, and acoustic emission characteristics. *Therm. Sci. Eng. Prog.* **2026**, *70*, 104507. [CrossRef]
4. Li, X.; Zhu, L.; Liu, J.; Cao, Z.; Xue, Y.; Dang, F. Fracture evolution and mechanical deterioration of granite under cyclic thermal and liquid nitrogen cryogenic impact. *Phys. Fluids* **2025**, *37*, 086652. [CrossRef]
5. Li, S.; Wang, C.; Yang, J.; Lai, Y.; Jiang, Q.; Wang, X. Thermo-hydro-mechanical process and damage mechanism of a cold-region canal under coupled wetting–drying and freezing–thawing cycles. *Acta Geotech.* **2022**, *17*, 4655–4665. [CrossRef]
6. Li, J. Mechanics Models of Frost-Heaving and the Research of Anti-Frost Heave Structure for Lining Canal. Ph.D. Thesis, Northwest A&F University, Yangling, China, 2009.
7. Jiang, H.; Wang, E.; Niu, F.; Han, H.; Liu, X.; Ren, Z. Experimental investigation on performance degradation of insulation materials induced by freeze–thaw cycles and its applications. *Constr. Build. Mater.* **2022**, *350*, 128844. [CrossRef]
8. Wang, Z.; Cao, C.; Yu, Q.; Shen, J.; Han, M.; Xia, W.; Sun, X.; Wang, Q. Uneven frost heave deformation in water conveyance channels in cold-arid regions: Experimental evidence and thermo-hydro-mechanical coupling analysis. *J. Rock Mech. Geotech. Eng.* **2025**, *17*, 7107–7126. [CrossRef]
9. *SL654-2014*; Code for Rational Service Life and Durability Design of Water Resources and Hydropower Projects. Ministry of Water Resources of the People's Republic of China: Beijing, China, 2012.
10. Ohmine, I.; Saito, S. Dynamical Behavior of Water; Fluctuation, Reactions and Phase Transitions. *Bull. Chem. Soc. Jpn.* **2021**, *94*, 2575–2601. [CrossRef]
11. Pei, W.; Zhou, J.; Lu, J.; Du, S.; Zhou, Y. Laboratory investigation on the control effect of a slope buried thermosyphon embankment in permafrost regions. *Cold Reg. Sci. Technol.* **2025**, *241*, 104702. [CrossRef]
12. Yu, F.; Luo, J.; Niu, F.; Lin, Z.; Li, B.; Mu, Y.; Ju, X.; Liu, M.; Yin, G.; Gao, Z.; et al. Spatiotemporal dynamics of retrogressive thaw slumps on the Qinghai-Tibet Plateau: Integrating UAV-LiDAR and GPR. *Landslides* **2025**, *22*, 3351–3363. [CrossRef]
13. Gao, C.; Guo, Y.; Han, Y.; Xu, L. Microstructure evolution and permeability of fine-grained loess subjected to freeze-thaw cycles. *Eng. Geol.* **2025**, *357*, 108326. [CrossRef]
14. Wu, D.; Ma, D.; Wang, C.; Liu, H.; Liu, X. Frost heave deformation and mechanism of canal with high groundwater table in seasonally frozen region. *Environ. Earth Sci.* **2023**, *82*, 583. [CrossRef]
15. Ge, J.; Yuan, Y.; Jiang, H.; Wang, Z.; Wang, Y.; Xiao, M. Mitigating frost damage in cold region canals: Performance evaluation of a two-layer geomembrane lining structure. *Geotext. Geomembr.* **2025**, *53*, 1458–1472. [CrossRef]
16. Chen, Y.; Huang, Y.; Cai, Z.; Su, A. Failure mechanism and treatment measures for expansive soil canals in cold regions: A case study of the Xinjiang Water Conveyance Canal in China. *Cold Reg. Sci. Technol.* **2023**, *216*, 103991. [CrossRef]
17. Cai, H.; Li, S.; Liang, Y.; Yao, Z.; Cheng, H. Model test and numerical simulation of frost heave during twin-tunnel construction using artificial ground-freezing technique. *Comput. Geotech.* **2019**, *115*, 103155. [CrossRef]
18. Fang, K.; Miao, M.; Tang, H.; Jia, S.; Dong, A.; An, P.; Zhang, B. Insights into the deformation and failure characteristic of a slope due to excavation through multi-field monitoring: A model test. *Acta Geotech.* **2023**, *18*, 1001–1024. [CrossRef]
19. Gao, J.; Lu, K.; Lai, Y.; Wang, K.; Ma, Q.; Li, Q.; Zhang, J.; Yuan, Y. Experimental and numerical investigations on novel assembled channel lining applied to seasonally frozen ground regions. *Cold Reg. Sci. Technol.* **2025**, *234*, 104475. [CrossRef]
20. Li, S.; Zhang, M.; Tian, Y.; Pei, W.; Zhong, H. Experimental and numerical investigations on frost damage mechanism of a canal in cold regions. *Cold Reg. Sci. Technol.* **2015**, *116*, 1–11. [CrossRef]
21. Jiang, H.; Liu, X.; Chen, Y.; Wang, E.; Fu, Q.; He, J.; Zhong, H. Model test investigation on heat and deformation behaviors of canal slopes with protective layers caused by freeze-thaw action. *Cold Reg. Sci. Technol.* **2024**, *228*, 104338. [CrossRef]

22. Wang, E.; Fu, Q.; Liu, X.; Li, T.; Li, J. Simulating and validating the effects of slope frost heaving on canal bed saturated soil using coupled heat-moisture-deformation model. *Int. J. Agr. Biol. Eng.* **2017**, *10*, 184–193.
23. Jiang, H.; Zhang, M.; Wang, Z.; Bai, R.; Sun, X.; Kong, X. Experimental investigation on the asymmetric heat-water-deformation behaviors between sunny and shady slopes in seasonally frozen regions. *Int. Commun. Heat Mass Transf.* **2024**, *158*, 107903. [CrossRef]
24. Li, Z.; Liu, X.; Sun, Y.; Jiang, X. Numerical simulation of frost heaving damage of earth-rock dam berms in cold regions with thermo-hydro-mechanical coupling. *Cold Reg. Sci. Technol.* **2024**, *223*, 104207. [CrossRef]
25. Wang, Z.; Zhang, M.; Li, G.; Liu, W. A mechanical model for trapezoidal canals lined with geomembranes and anti-slip material during freezing-thawing processes. *Cold Reg. Sci. Technol.* **2023**, *208*, 103783. [CrossRef]
26. Li, Z.; Liu, S.; Feng, Y.; Liu, K.; Zhang, C. Numerical study on the effect of frost heave prevention with different canal lining structures in seasonally frozen ground regions. *Cold Reg. Sci. Technol.* **2013**, *85*, 242–249. [CrossRef]
27. McRoberts, E.C.; Morgenstern, N.R. The stability of thawing slopes. *Can. Geotech. J.* **1974**, *50*, 447–469. [CrossRef]
28. Zheng, C.; Chao, W. Slope Stability Analysis Under Extreme Snow Weather. *Highw. Eng.* **2012**, *37*, 42–44+72.
29. Li, H.; Yu, L. Study on Subgrade Slope Stability under the Effect of Freeze-Thaw Cycle. *Subgrade Eng.* **2011**, *05*, 26–28+32.
30. Li, Z. Study on Mechanism of Moisture-Heat-Stress Coupling for Frozen Soil and Engineering Application. Master's Thesis, Harbin Institute of Technology, Harbin, China, 2017.
31. *GB/T50123-2019*; Standard for Geotechnical Testing Method. Minist. Hous. Urban-Rural Dev. China Planning Press: Beijing, China, 2019.
32. Zhu, L.; Li, D.; Guo, X. Simulitude analysis of modeling test for chargeless pressure in the freezing-thawing process of soil. *J. Glaciol. Geocryol.* **1993**, *15*, 166–169.
33. Xu, D. *Runoff Variation and It's Impaction Factor in Nenjiang River During 1956–2006*; Graduate School of the Chinese Academy of Sciences: Beijing, China, 2008.
34. Harlan, R. Analysis of coupled heat-fluid transport in partially frozen soil. *Water Resour. Res.* **1973**, *9*, 1314–1323. [CrossRef]
35. Xu, X.; Wang, J.; Zhang, L. *Physics of Frozen Soil*; Science Press: Beijing, China, 2001.
36. Taylor, G.S.; Luthin, J.N. A model for coupled heat and moisture transfer during soil freezing. *Can. Geotech. J.* **1978**, *15*, 548–555. [CrossRef]
37. Van Genuchten, M.T. A closed-form equation for predicting the hydraulic conductivity of unsaturated soils. *Soil. Sci. Soc. Am. J.* **1980**, *44*, 892–898. [CrossRef]
38. Gardner, W.; Hillel, D.; Beny, A.Y. Post-irrigation movement of soil water: Redistribution. *Water Resour. Res.* **1970**, *6*, 851–861. [CrossRef]
39. Bai, Q.; Li, X.; Tian, Y.; Fang, J. Equations and numerical simulation for coupled water and heat transfer in frozen soil. *Chin. J. Geotech. Eng.* **2015**, *37*, 131–136.
40. Li, Q. Study on Thermo-Hydro-Mechanical Coupling of Frozen Soil Around Oil Pipeline Under Freeze-Thaw Cycles. Master's Thesis, Southwest Petroleum University, Chengdu, China, 2019.
41. Wang, C. Research on Freeze-Thaw Slumping Mechanism of Harbin-Dalian High-Speed Railway Slope in Seasonally Frozen Soil Region. Master's Thesis, Harbin Institute of Technology, Harbin, China, 2014.
42. Gao, C.; Wei, R.; Chen, S. Centrifugal model tests on deformation of slopes reinforced with piles. *Chin. J. Geotech. Eng.* **2009**, *31*, 145–148.
43. Cai, Z.; Chen, H.; Huang, Y. Failure mechanism of canal slopes of expansive soils considering action of wetting-drying cycles. *Chin. J. Geotech. Eng.* **2019**, *41*, 1977–1982.
44. Cho, S.E. Effects of spatial variability of soil properties on slope stability. *Eng. Geol.* **2007**, *92*, 97–109. [CrossRef]
45. Gao, Z.; Wang, Y.; Liu, G. Effect of thermokarst lake on soil saturated hydraulic conductivity and analysis of its influenced factors. *Trans. Chin. Soc. Agric. Eng.* **2014**, *30*, 109–117.
46. Gao, Z.; Niu, F.; Lin, Z.; Luo, J.; Yin, G.; Wang, Y. Evaluation of thermokarst lake water balance in the Qinghai–Tibet Plateau via isotope tracers. *Sci. Total Environ.* **2018**, *636*, 1–11. [CrossRef]
47. Luo, J.; Yu, F.; Niu, F.; Yao, M.; Lin, Z.; Liu, M.; Yin, G.; Gao, Z. Recent rapid initiation and growth of retrogressive thaw slumps in the Hoh Xil region of the Qinghai-Tibetan Plateau. *Catena* **2024**, *243*, 108158. [CrossRef]
48. Scaringi, G.; Loche, M.A. Thermo-hydro-mechanical approach to soil slope stability under climate change. *Geomorphology* **2022**, *401*, 108108. [CrossRef]
49. Yang, N.; Ren, D.; Zheng, H.; Cao, Z.; Si, J.; Quan, L. Skeleton Structure of Segregated Ice Lenses in Frozen Soil and Its Effects on the Mechanical Properties. *J. Geotech. Geoenviron. Eng.* **2026**, *152*, 04025162. [CrossRef]
50. Jiang, H.; Niu, F.; Wang, E.; Ma, Q.; Cheng, L. Study on the thermophysical properties of clay under repeated freezing and thawing. *Pure Appl. Geophys.* **2020**, *177*, 5349–5366. [CrossRef]
51. Jiang, H.; Han, H.; Liu, X.; Wang, E.; Fu, Q.; Luo, J. Effect of repeated freeze-thaw cycles on mechanical properties of clay. *Heliyon* **2024**, *10*, e27261. [CrossRef]

52. Wang, R.; Jing, Z.; Luo, H.; Bao, S.; Jia, J.; Zhan, X. Effect of freeze–thaw cycles on root–Soil composite mechanical properties and slope stability. *PLoS ONE* **2024**, *19*, e0302409. [CrossRef] [PubMed]
53. Zhang, Z.; Su, Z.; Song, Z. Study on the microstructure of lateritic soil after freeze–thaw cycles under the background of climate warming. *Bull. Eng. Geol. Environ.* **2026**, *85*, 151. [CrossRef]
54. Ma, Y.; Su, P.; Zheng, Z.; Li, Y.; Liao, C. Progressive failure research of landslide based on strain softening of sliding zone soil. *J. Eng. Geol.* **2019**, *27*, 172–178.
55. Chen, Q.; Liu, Y.; Wang, Y.; Su, L.; Cheng, Y. Investigation of coupled thermo-hydro-mechanical processes on soil slopes in seasonally frozen regions. *Cold Reg. Sci. Technol.* **2025**, *229*, 104356. [CrossRef]